DOI:10.1190/image2023-3911109.1

Adaptive OCCAM's inversion for the interpretation of borehole ultra-deep azimuthal resistivity measurements

Wardana Saputra, Junsheng Hou, and Carlos Torres-Verdín, UT Austin; Sofia Davydycheva and Vladimir Druskin, 3D EM Modeling&Inversion JIP*

Summary

Ultra-deep azimuthal resistivity (UDAR) logging technology has been around for the last two decades. However, the real-time inversion of deep-sensing borehole electromagnetic measurements is still an outstanding challenge to yield a reliable image of subsurface electrical resistivity. In this study, we develop a new procedure for adaptive 1D inversion of UDAR measurements that quantifies the uncertainty of results and implements various measures of data misfit to trigger local higher-dimensional inversions. We construct an augmented linear system for fast and stable OCCAM's inversion that accounts for data and model weight matrices, as well as priors for adaptive inversion. We further verify the successful application of this adaptive inversion method on three resistivity models inspired by actual reservoir structures explored with commercial UDAR tool configurations.

Introduction

The development of deep-reading borehole resistivity measurements started in the last two decades with a lateral depth of investigation (DOI) up to 5 m (Seydoux et al., 2014). Today, the new generation of UDAR instruments include transmitter-receiver spacings that may exceed 30 m and operate at relatively low frequencies in the 1-100 kHz, which allows sensing tens of meters around the borehole (see Figure 1; Davydycheva et al., 2023). This technology represents a significant leap in imaging capabilities of subsurface structures, bridging the gap between two reservoir scales: near-wellbore logging and seismic interpretation (Antonsen et al., 2022). However, presence of thin layers, electrical anisotropy, complex borehole trajectory, multi-spacing and multi-frequency tool configurations makes the interpretation of raw UDAR measurements impossible without inversion (Pardo and Torres-Verdín, 2015).

To perform the inversion, a numerical simulator is required to model borehole resistivity measurements assuming a specific instrument configuration, which is often referred to as "forward model". Several 3D numerical simulators for UDAR measurements are available by solving the boundary-value problem of Maxwell's equation using finite differences or finite elements (Zhang et al., 1995; Davydycheva, and Druskin, 1999; Wang and Fang, 2001; Davydycheva et al., 2003, 2023; Hou and Torres-Verdín, 2003; Hou et al., 2006, Pardo and Torres-Verdín, 2021). Despite the availability of 3D forward models, the oil subsurface energy industry rarely makes use of 3D inversion results, especially in real-time during well navigation. Performing thousands of 3D finite-difference or finite-element simulations during 3D inversion comes with a significant computational cost, even with the advancements in modern computer architectures. Moreover, tackling a complex 3D structure leads to a higher number of unknowns, resulting in an excessively large system of linear equations, which further adds to the computational expense. To achieve real-time inversion results, many subsurface service and operating companies use faster 1D semi-analytical solutions of piecewise transversely isotropic resistivities (Gao and Torres-Verdín, 2003; Pardo and Torres-Verdín, 2015, Antonsen et al., 2022; and Davydycheva et al., 2023). Certainly, a trade-off exists between speed and accuracy when employing reduced-order modeling techniques. In this study, we develop a new adaptive inversion method that improves the accuracy of rapid 1D inversion based on the modification of the traditional OCCAM's algorithm (Constable et al., 1987, deGroot-Hedlin and Constable, 1990). We also show that the calculation of data misfit and uncertainty of inversion results is important to construct a reliable inversion prior, in addition to securing better interpretations of UDAR inversion results.

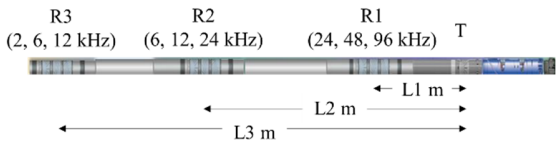

Figure 1: A typical commercial UDAR instrument consists of one transmitter and two or three receivers spaced by 7 – 32 m (Antonsen et al., 2022; Davydycheva et al., 2023). In this study, we define three instrument configurations as follows: 1) Type I: Three receivers (R1, R2, and R3) with spacings 7, 17, and 30 m, respectively, 2) Type II: Three receivers (R1, R2, and R3) with spacings 12.5, 19.8, and 32 m, respectively, and 3) Type III: Two receivers (R1 and R2) with spacings 13.1 and 25.3 m, respectively.

Method

We start by defining the following quadratic cost function to guide the inversion (Torres-Verdín and Habashy, 1993, 1995; Torres-Verdín et al., 2000):

$$C(\mathbf{m}) = \left\| \mathbf{W}_{\mathrm{d}} \cdot \left[\mathbf{d}(\mathbf{m}) - \mathbf{d}^{\mathrm{obs}} \right] \right\|^2 + \alpha^2 \left\| \mathbf{W}_{\mathrm{m}} \cdot [\mathbf{m} - \mathbf{m}_{\mathrm{R}}] \right\|^2 \quad (1)$$

Both $\mathbf{d}^{\mathrm{obs}}$ and $\mathbf{d}(\mathbf{m})$ are the vectors of observed and simulated measurements, respectively, which can be in the

form of magnetic field, voltage, apparent resistivity, or phase and attenuation (geosignals, e.g. Davydycheva, 2020); $\mathbf{m}$ and $\mathbf{m}_{\mathrm{R}}$ are the vector of model parameters and reference parameters, respectively, which consist of logarithmic resistivities and anisotropy ratios of each 1D layer, and general dip and azimuth for all layers. $\mathbf{W}_{\mathrm{d}}$ is the data weighting matrix, which is a diagonal matrix of the standard deviation of observed data noise for different tool configurations, while $\mathbf{W}_{\mathrm{m}}$ is the model weighting matrix that can be an identity matrix (Tikhonov), or first- and second-order derivatives with respect to true vertical depth.

We then implement OCCAM's inversion algorithm to iteratively minimize the quadratic cost-function in equation (1), yielding the following augmented linear systems, that need to be solved at each iteration-k:

$$\mathbf{m}_{k+1} = \mathbf{A}^{-1}\mathbf{b}, \tag{2}$$

$$\mathbf{A} = \begin{bmatrix} \mathbf{W}_{\mathrm{d}} \cdot \mathbf{J}(\mathbf{m}_k) \\ \alpha \mathbf{W}_{\mathrm{m}} \end{bmatrix}, \qquad \mathbf{b} = \begin{bmatrix} \mathbf{e} + \mathbf{r} \\ 0 \end{bmatrix}, \tag{3}$$

$$\mathbf{e} = \mathbf{W}_{\mathrm{d}} \cdot \left[\mathbf{J}(\mathbf{m}_k) \cdot \mathbf{m}_k - \left(\mathbf{d}(\mathbf{m}) - \mathbf{d}^{\mathrm{obs}}\right)\right], \tag{4}$$

$$\mathbf{r} = \left[\mathbf{J}^{\mathrm{T}}(\mathbf{m}_k) \cdot \mathbf{W}_{\mathrm{d}}^{\mathrm{T}}\right]^{-1} \cdot \left[\boldsymbol{\alpha}_{\boldsymbol{R}} \mathbf{W}_{\mathrm{m}}^{\mathrm{T}} \cdot \mathbf{W}_{\mathrm{m}} \cdot \mathbf{m}_{\mathrm{R}}\right]. \tag{5}$$

The Jacobian matrix, $\mathbf{J}$, is first obtained using finite difference, as follows:

$$\mathbf{J}(\mathbf{m}_k) = \frac{\partial \mathbf{d}(\mathbf{m}_k)}{\partial \mathbf{m}_k} \approx \frac{\mathbf{d}(\mathbf{m}_k + \mathbf{h}) - \mathbf{d}(\mathbf{m}_k)}{\mathbf{h}}, \tag{6}$$

where $\mathbf{h}$ is the small perturbation (e.g. 0.5–1 %) of model parameter, $\mathbf{m}$. After the first few iterations, the Jacobian matrix, $\mathbf{J}$, can also be approximated using Broyden's update (see Torres-Verdín et al., 2000), to further accelerate the inversion.

The regularization parameter, α, is calculated at every iteration-k to balance the linear equation in (3) as follows:

$$\alpha = \frac{\|\mathbf{W}_{\mathrm{d}} \cdot \mathbf{J}(\mathbf{m}_k)\|}{\|\mathbf{W}_{\mathrm{m}}\|}. \tag{7}$$

To add flexibility of giving variable weights to the reference model, we calculate $\boldsymbol{\alpha}_{\boldsymbol{R}}$ as follows:

$$\boldsymbol{\alpha}_{\boldsymbol{R}} = \mathrm{diag}(\boldsymbol{w}), \qquad 1 \le w_j \le \alpha^2. \tag{8}$$

Notice that the value of w_j for the reference model $m_{R,j}$ is α^2 for the maximum weight and 1 for the minimum weight.

The systems of linear equations in (2) – (8) improve the condition number of the inverted matrix and are relatively more stable than the traditional OCCAM's formulation. Vector $\mathbf{r}$ contains the model reference (prior) term that is fundamental for adaptive inversion.

Upon convergence, based on Cramer-Rao's inequality (Habashy and Abubakar, 2004), we calculate the model covariance matrix, $\boldsymbol{\Sigma}_{\mathrm{m}}$, as the inverse of the Hessian matrix from the quadratic cost-function in (1), as follows:

$$\boldsymbol{\Sigma}_{\mathrm{m}} \approx \left[2\mathbf{J}^{\mathrm{T}}(\mathbf{m}_k) \cdot \mathbf{W}_{\mathrm{d}}^{\mathrm{T}}\mathbf{W}_{\mathrm{d}} \cdot \mathbf{J}(\mathbf{m}_k) + 2\alpha^2 \mathbf{W}_{\mathrm{m}}^{\mathrm{T}} \cdot \mathbf{W}_{\mathrm{m}}\right]^{-1}, \tag{9}$$

where the standard deviation of the model parameters, $\boldsymbol{\sigma}_{\mathrm{m}}$, can be approximated as the square root of the diagonal of matrix $\boldsymbol{\Sigma}_{\mathrm{m}}$, and finally, the model uncertainty is calculated as

$$\mathbf{u}_{\mathrm{m}} = \frac{\boldsymbol{\sigma}_{\mathrm{m}}}{\mathbf{m}} \times 100\%. \tag{10}$$

Meanwhile, the data misfit is calculated as the variance ratio between data error and observed data, i.e.,

$$\boldsymbol{\delta}_{\mathrm{d}} = \frac{\mathrm{var}\left(\mathbf{W}_{\mathrm{d}}\left[\mathbf{d}(\mathbf{m}) - \mathbf{d}^{\mathrm{obs}}\right]\right)}{\mathrm{var}(\mathbf{W}_{\mathrm{d}}[\mathbf{d}^{\mathrm{obs}}])} \times 100\%. \tag{11}$$

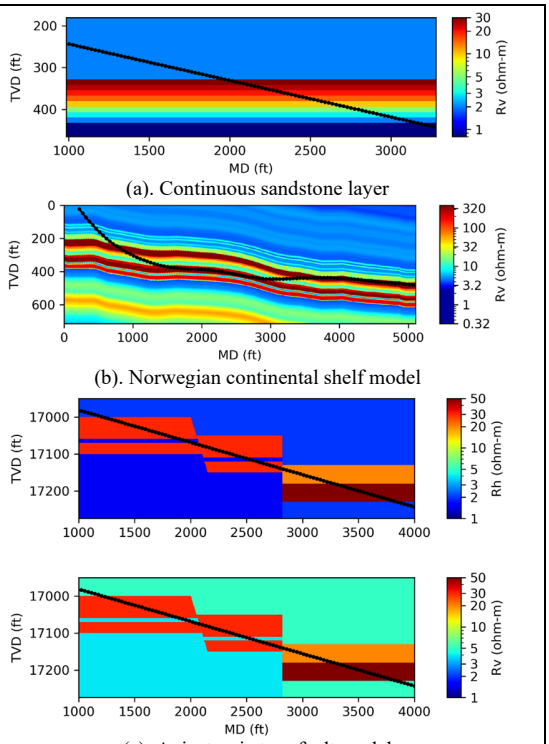

(a). Continuous sandstone layer

(b). Norwegian continental shelf model

(c). Anisotropic two-fault model

Figure 2: Three resistivity models inspired by actual subsurface reservoir structures. Models (a) and (b) are adapted from Antonsen et al., (2022), while the anisotropic model (c) is obtained from Davydycheva et al., (2023). Models (a) and (c) have a well trajectory with a constant inclination at 85°, while model (b) has a variable inclination and azimuth along the trajectory.

Briefly, our full inversion method works as follows: First, for each logging point, we perform a 0D inversion to estimate a local homogeneous resistivity model. We then use the 0D resistivity result as a reference model for 1D inversion (first-pass). Besides the resistivity curtain, we also output the model uncertainty curtain and data misfit curves. To adjust the lateral continuity of 1D inversion results, we

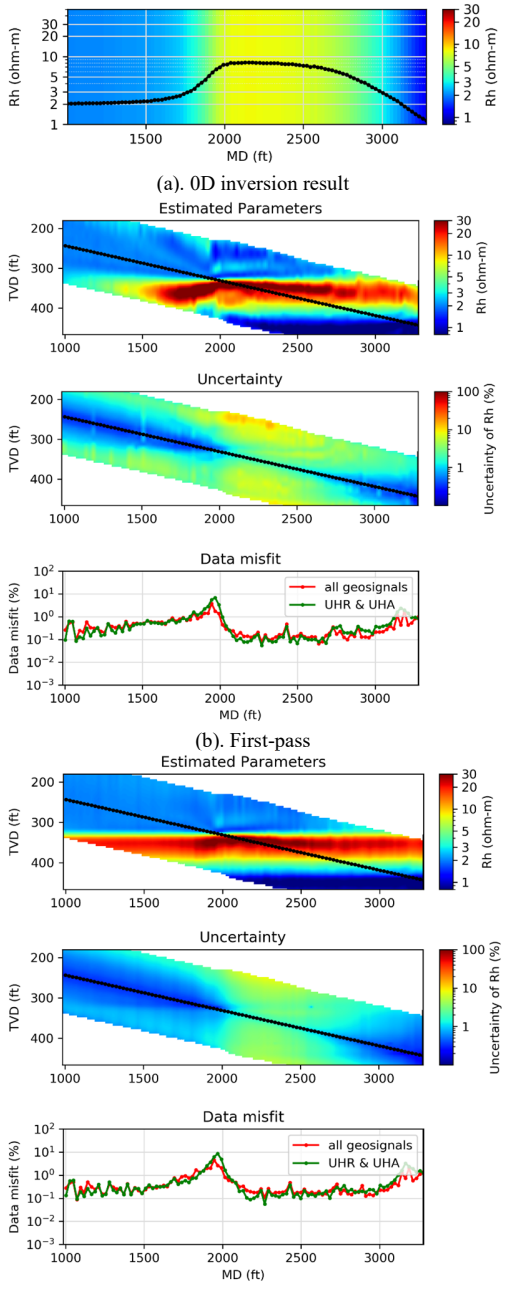

Figure 3: Inversion results obtained for the first model. (a) 0D inversion, (b) First-pass inversion with prior from 0D inversion. (c) Second-pass inversion with prior from the first-pass. Besides the 2D curtain of estimated parameters, we also display the model uncertainty and data misfit for the 1D inversion results.

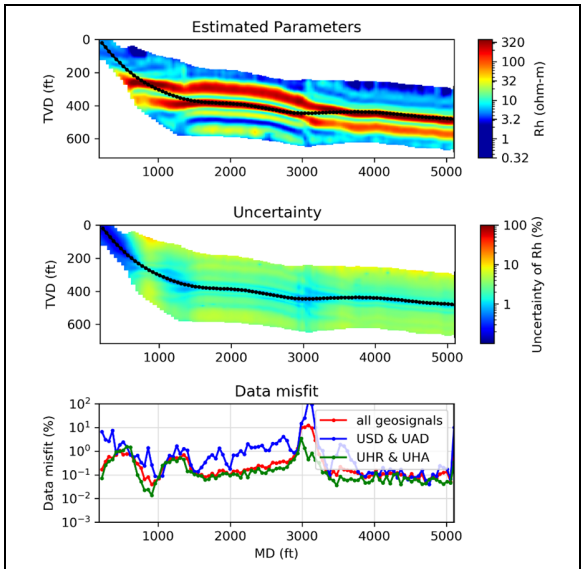

Figure 4: Second-pass inversion results for the second model (Norwegian continental shelf model) consist of estimated parameters, model uncertainty and data misfit for all logging points.

apply a weighted sliding window in which the weight is inversely proportional to the model uncertainty and data misfit (see the Appendix). Finally, we use the post-processed result from the first-pass inversion to implement adaptive 1D inversion.

Results

We show how the adaptive OCCAM inversion method improves 1D inversion results based on three different synthetic resistivity models, as shown in Figure 2, with instrument configurations detailed in Figure 1 (Type I: model-a, Type II: model-b, Type III: model-c). The 3D forward model from Davydycheva et al., (2023) is used to generate the synthetic phase and attenuation measurements.

The first model (Figure 2a) is inspired by a continuous sandstone layer in between two less resistive shale layers. The gradation of resistivity in the sandstone layer mimics the alternation between oil- and water-bearing formations. A directional well with a constant inclination of 85° penetrates the continuous layer. Figure 3 shows inversion results obtained for the first model (Figure 2a). First, we run 0D inversion for each of the 100 logging points (Figure 3a), and typically we find that the data misfits are high elsewhere (>10%) except at places where the tool senses a homogeneous resistivity background. In Figure 3b, we run the piecewise 1D inversion for each log point with a prior from 0D inversion. We observe that the data misfit decreases significantly for all logging points. Additionally, we plot the

DOI:10.1190/image2023-3911109.1

uncertainty of inversion results, which monotonically increases away from the wellbore. Next, we apply a weighted sliding window based on both data misfit and uncertainty to the first-pass inversion result and made it a prior for the second-pass inversion (Figure 3c). This example shows a typical result obtained for UDAR inversion where the continuous sandstone layer appears as a discontinuous wedge layer due to instrument/measurement limitations (first-pass). The adaptive inversion (second-pass) displays a better result which is closer to the true model, and gives rise to both lower uncertainty and lower data misfit. The remaining two models exhibit more spatially complex geological structures, where the second model (Figure 2b) is from a reservoir on the Norwegian continental shelf with significant resistivity contrasts, numerous thin layers, and a complex well trajectory. The third model (Figure 2c) is also inspired by an actual hydrocarbon reservoir discontinued by two major faults, where well inclination is 85° and the well trajectory penetrates the two faults. Some of the layers included in the second and third models are thinly laminated and anisotropic, making the inversion more challenging. Nevertheless, our adaptive inversion method successfully yields good results, especially after the first-pass (see Figures 4 and 5). In addition, our adaptive inversion method is fast and only requires 10 – 50 CPU seconds to yield the 2D curtain of resistivity and model uncertainty, and data misfit for all logging points, on a standard personal computer with 8 cores.

Conclusions

To our knowledge, this is the first technical paper that highlights the significance of adaptive inversion for improving 1D inversion results of UDAR measurements. We also showed that the calculated uncertainty and data misfit are beneficial to construct a prior model for the adaptive inversion. The developed method is the base of multi-dimensional inversion where we start with the lowest dimension (0D) before moving to higher dimensions (1D, 2D, and 3D) to progressively decrease data misfit with reliable measures of spatial smoothness and based on acceptable uncertainty of inversion results.

Acknowledgments

The work was supported by the University of Texas at Austin's Deep Imaging Sub-Consortium of the FE consortium, currently sponsored by AkerBP, Baker Hughes, BP, ENI, Equinor ASA, Halliburton, and SLB.

Appendix: Construction of the Adaptive 1D Inversion Prior

1D inversion assumes numerous piecewise 1D models along the well trajectory. Therefore, the 2D resistivity curtain from 1D inversion results often lacks lateral continuity. To improve inversion results, we perform a post-processing process for each of model parameters, $m_{i,j}$, in the 2D curtain using equation (12), i.e.,

$$\bar{m}_{i,j} = \exp\left(\frac{\sum_{k=j-n}^{k=j+n} w_k \ln m_{i,k}}{\sum_{k=j-n}^{k=j+n} w_k}\right),$$
$$w_k = \frac{1}{u_{m_{i,k}} \times \delta_{d,k}}, \qquad n = \frac{L}{dx}. \tag{12}$$

The weight, w_k, is calculated from corresponding model uncertainty and data misfit, while n is the pixel range of the geometric mean, which is the ratio between a certain length, L (ft), and logging interval, dx (ft).

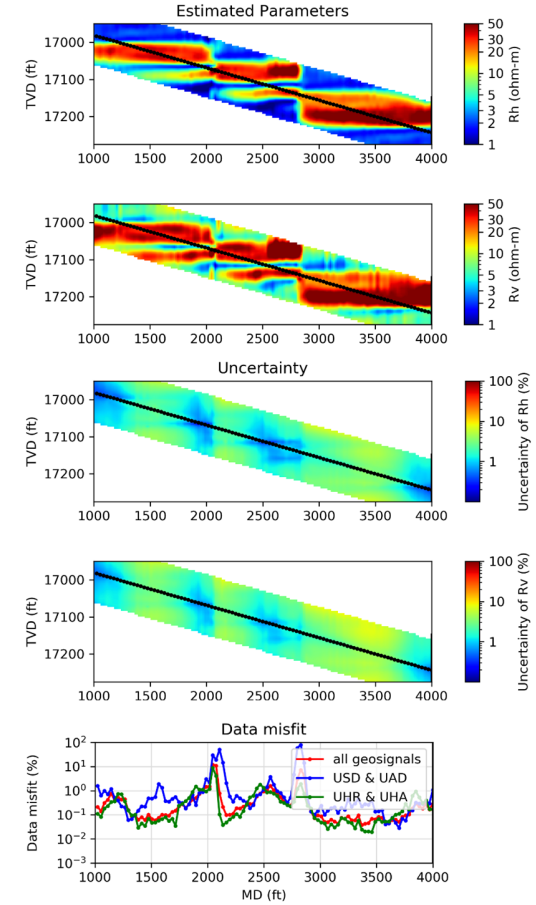

Figure 5: Second-pass inversion results for the third model (Anisotropic two-fault model) include estimated parameters and model uncertainty for both horizontal and vertical resistivities, as well as data misfit.

REFERENCES

Antonsen, F., B. E. Danielsen, K. R. Jensen, M. Prymak-Moyle, J. K. Lotsberg, M. E. T. De Oliveira, and M. V. Constable, 2022, What Next After a Decade with Significant Advances in the Application of Deep Directional Measurements?: Presented at the 63th Annual Logging Symposium, SPWLA, doi: https://doi.org/10.30632/SPWLA-2022-0047.

Constable, S. C., R. L. Parker, and C. G. Constable, 1987, Occam's inversion: A practical algorithm for generating smooth models from electromagnetic sounding data: Geophysics, **52**, 289–300, doi: https://doi.org/10.1190/1.1442303.

Davydycheva, S. and V. Druskin, 1999, Staggered grid for Maxwell's equations in 3-D anisotropic media, *in* M. Oristaglio and B. Spies, eds., Three-Dimensional Electromagnetics: SEG, 138–145, doi: https://doi.org/10.1190/1.9781560802154.ch9.

Davydycheva, S., V. Druskin and T. Habashy, 2003, An efficient finite-difference scheme for electromagnetic logging in 3D anisotropic inhomogeneous media: Geophysics, **68**, 1525–1536, doi: https://doi.org/10.1190/1.1620626.

Davydycheva, S., V. Druskin, L. Knizhnerman, and M. Rabinovich, 2020, Quality control of ultra-deep resistivity imaging using fast 3D electromagnetic modeling: 90th Annual International Meeting, SEG, Expanded Abstracts, 380–384, doi: https://doi.org/10.1190/segam2020-3425809.1.

Davydycheva, S., C. Torres-Verdín, J. Hou, W. Saputra, M. Rabinovich, F. Antonsen, B.E. Danielsen, V. Druskin, and J. Zimmerling, 2023, 3D electromagnetic modeling and quality control of ultradeep borehole azimuthal resistivity measurements, Presented at the 64th Annual Logging Symposium, SPWLA, doi: https://doi.org/10.30632/SPWLA-2023-0070.

deGroot-Hedlin, C., and S. Constable, 1990, Occam's inversion to generate smooth, two-dimensional models from magnetotelluric data: Geophysics, **55**, 1613–1624, doi: https://doi.org/10.1190/1.1442813.

Gao, G. Z., and C. Torres-Verdín, 2003, Fast inversion of borehole array induction data using an inner-outer loop optimization technique: Presented at the 44th Annual Logging Symposium, SPWLA.

Habashy, T., and A. Abubakar, 2004, A general framework for constraint minimization for the inversion of electromagnetic measurements: Progress in Electromagnetics Research, **46**, 265–312, doi: https://doi.org/10.2528/PIER03100702.

Hou, J., and C. Torres-Verdín, 2003, Finite-difference modeling of EM fields using coupled potentials in 3D anisotropic media: application to borehole logging: 73rd Annual International Meeting, SEG, Expanded Abstracts, 522–525, doi: https://doi.org/10.1190/1.1817977.

Hou, J., R. K. Mallan, and C. Torres-Verdín, 2006, Finite-difference simulation of borehole EM measurements in 3D anisotropic media using coupled scalar-vector potentials: Geophysics, **71,** G225–G233, doi: https://doi.org/10.1190/1.2245467.

Pardo, D., and C. Torres-Verdín, 2015, Fast 1D inversion of logging-while-drilling resistivity measurements for improved estimation of formation resistivity in high-angle and horizontal wells: Geophysics, **80**, no. 2, E111–E124, doi: https://doi.org/10.1190/geo2014-0211.1.

Pardo, D., P. J. Matuszyk, V. Puzyrev, C. Torres-Verdin, M. J. Nam, and V. M. Calo, 2021, Modeling of resistivity and acoustic borehole logging measurements using finite element methods: Elsevier.

Seydoux, J., E. Legendre, E. Mirto, C. Dupuis, J. M. Denichou, N. Bennett, G. Kutiev, M. Kuchenbecker, C. Morriss, and L. Yang, 2014, Full 3D deep directional resistivity measurements optimize well placement and provide reservoir-scale imaging while drilling, Presented at the 55th Annual Logging Symposium, SPWLA.

Torres-Verdín, C., and T. M. Habashy, 1993, Cross-well electromagnetic tomography: Presented at the 3rd International Congress of the Brazilian Geophysical Society, European Association of Geoscientists & Engineers.

Torres-Verdín, C. and T.M. Habashy, 1995. A two-step linear inversion of two-dimensional electrical conductivity: IEEE Transactions on Antennas and Propagation, **43**, 405–415, doi: https://doi.org/10.1109/8.376039.

Torres-Verdín, C., V. L. Druskin, S. Fang, L. A. Knizhnerman, and A. Malinverno, 2000, A dual-grid nonlinear inversion technique with applications to the interpretation of dc resistivity data: Geophysics, **65**, 1733–1745, doi: https://doi.org/10.1190/1.1444858.

Wang, T., and S. Fang, 2001, 3-D electromagnetic anisotropy modeling using finite differences: Geophysics, **66**, 1386–1398, doi: https://doi.org/10.1190/1.1486779.

Zhang, J., R. L. Mackie, and T. R. Madden, 1995, 3-D resistivity forward modeling and inversion using conjugate gradients: Geophysics, **60**, 1313–1325, doi: https://doi.org/10.1190/1.1443868.